Contents lists available at ScienceDirect

Photonics and Nanostructures - Fundamentals and Applications

journal homepage: www.elsevier.com/locate/photonics

Optical nonlinearities of mercury telluride quantum dots measured by nanosecond pulses

R.A. Ganeev [a,b,c,*], I.A. Shuklov [d], A.I. Zvyagin [a], A. Mardini [d], A.A. Lizunova [d], G.S. Boltaev [c], I.B. Sapaev [c], V.V. Kim [b], O.V. Ovchinnikov [a], V.F. Razumov [d,e]

[a] Department of Physics, Voronezh State University, Voronezh 394006, Russia
[b] Institute of Astronomy, University of Latvia, Riga LV-1004, Latvia
[c] Tashkent Institute of Irrigation and Agricultural Mechanization Engineers, National Research University, Kori Niyozov street 39, Tashkent 100000, Uzbekistan
[d] Moscow Institute of Physics and Technology (National Research University), Dolgoprudny 141701, Russia
[e] Institute of Problems of Chemical Physics, Russian Academy of Sciences, Chernogolovka 142432, Russia

ARTICLE INFO

ABSTRACT

We synthesized the colloidal mercury telluride quantum dots (QDs) and analyzed their low-order nonlinear optical properties using 1064 nm and 532 nm, 10 ns pulses. HgTe QDs colloidal suspension showed the strong saturable absorption and negative nonlinear refraction (saturation intensity $I_{SA} = 5 \times 10^8$ W cm^{-2}, nonlinear absorption coefficients attributed to saturable absorption and reverse saturable absorption $\beta_{SA} = -4 \times 10^{-9}$ cm W^{-1} and $\beta_{RSA} = 1 \times 10^{-8}$ cm W^{-1}, nonlinear refractive index $\gamma = -6 \times 10^{-13}$ cm^2 W^{-1}) while using the 532 nm probe pulses. The nonlinear optical parameters of this suspension at 1064 nm were smaller (nonlinear absorption coefficient attributed to the two-photon absorption $\beta_{2PA} = 6 \times 10^{-10}$ cm W^{-1}, $\gamma = -5 \times 10^{-14}$ cm^2 W^{-1}). The negative nonlinear refraction of HgTe QDs was attributed to the thermal and Kerr effects in the case of 532 nm and 1064 nm probe pulses, respectively.

1. Introduction

Mercury telluride is a semimetal under bulk form with zinc-blend crystal structure. HgTe colloidal quantum dots (CQDs) are among of the most promising materials for mid-IR applications [1]. It is expected that application of HgTe CQDs will make mid-IR sensing less expensive and more efficient even by room temperature [2]. Possible multi-exciton generation is another interest for these materials under colloidal form [3]. Owing to its unique properties, this material has drawn attention as part of ongoing studies of chemistry and physical properties of the chalcogenide CQDs [4–6].

Among the physical properties of these CQDs, the nonlinear optical characterization can be considered as a rout towards the application of mercury telluride quantum dots (HgTe QDs) as the media for efficient high-order harmonics generation. Previously, the application of metal sulfide QDs as the emitters of high-order harmonics of ultrashort laser pulses allowed achieving the efficient conversion of IR emission of Ti: sapphire lasers towards the shorter-wavelength region ($\lambda < 50$ nm).

A search for advanced QDs allowing efficient harmonics generation will open the door for the application of generating radiation of harmonics in different fields of physics and chemistry, while also provides the opportunity in the analysis of the optical properties of QDs using high-order nonlinear spectroscopy methods. One can suggest that the higher-order nonlinear optical response of materials can be directly related to the low-order nonlinear susceptibility of these species. The analysis of the low-order nonlinear optical processes, like nonlinear refraction and nonlinear absorption, in these materials would allow determining the potentially attractive QDs for high-order harmonics generation. In most cases, the ablation of such QDs for plasma formation was carried out using nanosecond laser pulses. Thus, the use of similar pulses for analysis of nonlinear refraction, nonlinear absorption, and other lower-order nonlinear optical processes can provide information about the usefulness of QDs for harmonic generation, as well as in photonics and optoelectronics.

Mercury telluride QDs are of great interest in comparison with nonlinear optical crystals due to the possibility of controlling the nonlinear optical properties by varying the parameters of such QDs like size and shape. Both the spectral properties of this material and the effects of the local field, which are widely discussed in the scientific literature, depend on these parameters. The optical characteristics of

---

* Corresponding author at: Department of Physics, Voronezh State University, Voronezh 394006, Russia.
E-mail addresses: rashid.ganeev@lu.lv (R.A. Ganeev), shuklov.ia@mipt.ru (I.A. Shuklov).

these QDs allow them to use as IR detectors, passive mode-lockers and optical switches. To efficiently use the mercury telluride quantum dots in above applications, one has to determine their nonlinear optical characteristics. Meanwhile the nonlinear optical properties of HgTe nanocrystals were scarcely investigated. Some nonlinear properties of bulk material were demonstrated long time ago [7]. They have reported that mercury telluride is shown to have the largest known third-order nonlinear optic susceptibility with response time in the picosecond range. At 10.6 μm and $T = 300$ K, its third-order nonlinear susceptibility was determined to be $\chi^{(3)} = 1.6 \times 10^{-4}$ esu. As for the QDs, the only study was reported where the picosecond and femtosecond pulses were used for determination of the nonlinear optical properties of these QDs [8].

The analysis of nonlinear refraction, saturable absorption (SA), reverse saturable absorption (RSA), and two-photon absorption (2PA) using long (nanosecond) pulses can reveal the peculiarities of those processes in QDs, which could not be revealed using the short laser pulses. Here, we report the synthesis of HgTe QDs and analyze their nonlinear optical properties using 10 ns pulses at two wavelengths of laser radiation (1064 and 532 nm).

2. Synthesis of HgTe CQDs

The preparation of mercury telluride with narrow size-distribution was performed by applying the hot-injection method. We applied the method based on the tellurium precursor prepared from *n*-trioctylphosphine and elemental tellurium [9,10]. The reaction of this tellurium precursor with mercury halides requires significantly lower temperatures (60–80 °C) than with cadmium or zinc (200–300 °C) for the preparation of telluride nanocrystals. The small-sized HgTe CQDs capped with 1-dodecanethiol were prepared by short reaction times at the temperature of 60 °C. It was found that the amine-thiol ligand exchange is not complete under applied conditions of synthesis and a certain amount of oleylamine remains in the ligand shell. The obtained colloidal solutions showed a good colloidal stability.

The typical synthesis of HgTe CQDs was performed by mixing of two precursors. The tellurium precursor was prepared by dissolution of 0.381 g (3 mmol) of Te powder in 3 ml (6.7 mmol) of trioctylphosphine at 90 °C under continuous Ar flow. The solution of Te dissolved in trioctylphosphine was obtained after 1 h. Mercury precursor was prepared as following: 60 mg of $HgCl_2$ was dissolved in 8 ml of dry oleylamine at 100 °C under continuous argon flow for 1 h. The resulting solution was cooled to 60 °C. Then 0.2 ml of tellurium precursor was rapidly injected by syringe under Ar. The reaction was stirred for 15 min at 60 °C. The quenching mixture consisted of 16 ml of tetrachloroethylene (TCE), 3.1 ml of (0.8 mmol) dodecanthiol (DDT) and 1.5 ml of trioctylphosphine was added to the reaction mixture and the resulting solution cooled down to the room temperature. The HgTe nanocrystals were isolated by adding 4 ml of methanol per 6 ml of the resulting solution followed by centrifugation. The resulting precipitate was redispersed in 2 ml of TCE. 2 ml of acetonitrile was added to the resulting solution. The precipitate was dried under Ar and redispersed in 1 ml of TCE. Finally, the resulting solution was filtered using a 0.22 μm hydrophobic polytetrafluoroethylene syringe filter.

The HgTe could be oxidized with oxygen of air. Correspondingly, the oxidation products could affect the results of nonlinear optical experiments. We carefully analyzed the chemical composition of HgTe QDs by X-ray photoelectron spectroscopy (XPS) and X-ray diffraction (XRD) in order to confirm the purity of the samples. XPS is the most informative method to determine the chemical composition of nanocrystals. The chemical compositions were explored by XPS (PHOIBOS 150 MCD, Specs). The high-resolution XPS spectrum confirmed that the main constituent of monocrystalline core was HgTe. The crystal structure was identified by XRD (Thermo Fisher Scientific Inc.). Zinc blend structure of HgTe CQD without traces of other phases was observed by XRD. This phase could be observed in natural HgTe mineral, namely coloradoite. In

our case, we did not observe any compounds of Te^{4+} like $HgTeO_3$ or TeO_2 (paratellurite), which typical for the heavily oxidized HgTe samples (Fig. 1a).

The Fourier-transform infrared spectroscopy (FTIR, Spectrum 100, Perkin Elmer) was used at infrared range (5000–1000 cm^{-1}) to investigate the ligand shell of nanoparticles. The CQDs were dried on the Ge plate. The presence of 1-dodecanethiol was confirmed by FTIR. C-H stretching of methyl and methylene groups could be observed at 2924 cm^{-1} and 2850 cm^{-1}, as well as 1465 cm^{-1} (Fig. 1b). The signals of free thiol were not observed in the FTIR spectrum.

The HgTe CQDs with the first absorption peak at 1412 nm (Fig. 1c) were isolated after 15 min. It should be noted that the observed apparent maximum corresponding to the most probable exciton transition in the optical absorption has a rather small half-width, not exceeding 0.15 eV. This means that we observed a quantum-dimensional effect in the optical absorption spectrum of HgTe QDs. The contribution to the observed spectrum from elastic Rayleigh scattering is minimal.

The Raman spectrum (DXR Raman microscope ThermoFisher Scientific, a Si detector, and a 785 nm laser excitation) of a thin film, obtained by drop-casting of HgTe colloidal QD on glass substrate, was recorded in the 50–500 cm^{-1} range (Fig. 1d). The observed three lines were attributed to the longitudinal acoustic (LA) phonon at 91.3 cm^{-1}, the transverse optic (TO) phonon at 116 cm^{-1} and the longitudinal optic (LO) phonon at 138 cm^{-1}. A weak peak around 260 cm^{-1} is considered to be a harmonic of the previous peaks. It is consistent with earlier reported Raman spectra of CQDs HgTe samples [11].

SEM images were not retrieved, since we analyzed only the colloidal solutions. Obtaining film structures and their analysis were beyond the scope of this study.

The samples of larger QDs could be obtained by longer reaction times, for example, HgTe CQDs with the first absorption peak at 1560 nm after 60 min and at 1631 nm after 90 min. The observed absorption peaks were significantly broader (about 260 nm) in both larger samples and therefore a size-distribution expected to worsen. Due to the smallest size among the synthesized samples, the colloidal HgTe nanocrystals prepared at 60 °C during 15 min reaction time were used for further investigation.

The morphological and structural features of the synthesized nanoparticles were investigated by a transmission electron microscope (TEM, JEM-2100, JEOL). TEM allowed determining the mean size of 4 nm (Fig. 1e) that fits well with the observed first absorption peak at 1412 nm according to the date previously reported for spherical HgTe nanoparticles [12,13]. Fig. 1f shows the large area filled in by the QDs.

The material properties, namely a small size (~4 nm) and a low electron density of the studied quantum dots, can cause the low contrast of TEM images. The low contrast of TEM images was also due to the high affinity of the organic ligands used for QDs synthesis to induce an agglomeration. The scattering from agglomerates of nanoparticles and organic ligands reduces the contrast of TEM and makes it impossible to see the sharp image of nanocrystals. However, complete removal of these ligands is an arduous task. It could lead to even greater sintering of nanoparticles when recording TEM images. The using of carbon film with the thickness comparable to the particle size makes technically problematical to obtain images with better contrast of such small objects. The studied nanoparticles do not have the ideal spherical shape. Since the quantum dots have a crystal structure thus a spherical shape is not favored.

3. Nonlinear optical studies of HgTe CQDs

Studies of the nonlinear optical properties of our samples were performed using the standard Z-scan technique (inset to Fig. 2a). The main idea of this technique is to measure the change in incident Gaussian laser beam intensity during transmission through the sample as a function of its position (z-position) with regard to the focal plane of the beam. Transmitted beam is collected by means of two detector arrangements:
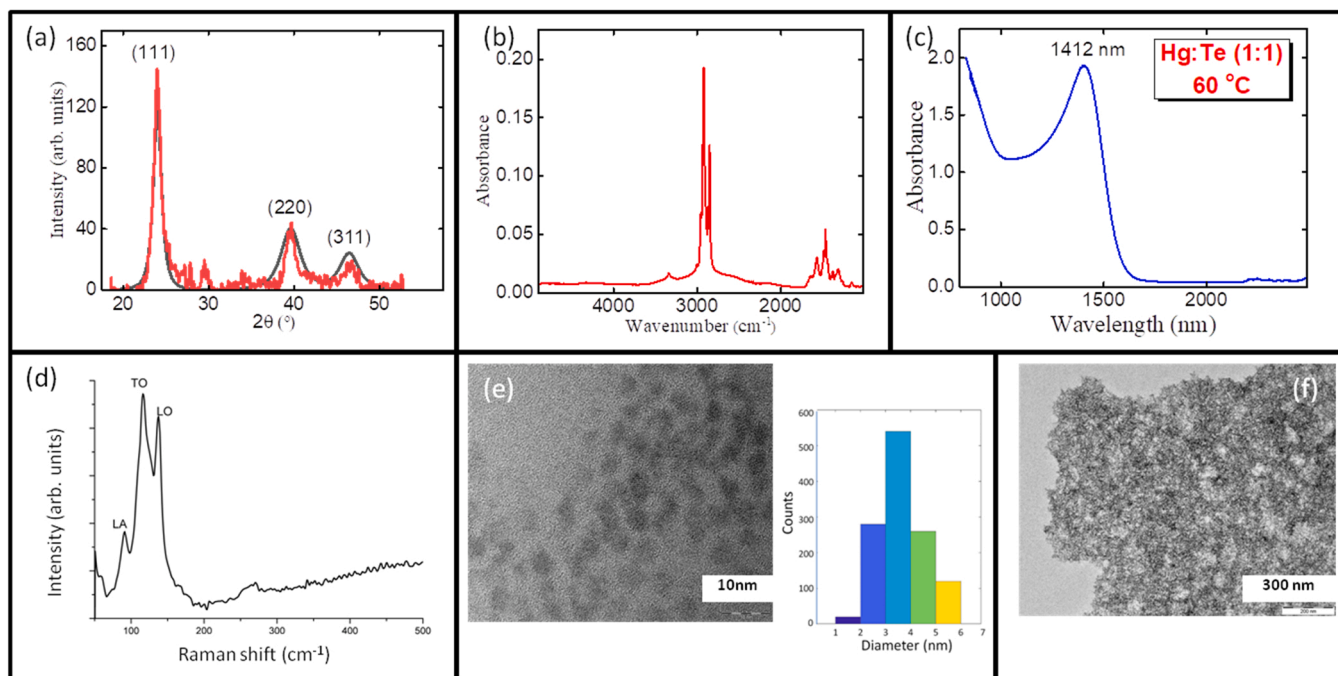
Fig. 1. Characterization of HgTe QDs. (a) XRD of synthesized QDs. (b) Fourier-transform infrared spectrogram. (c) Absorption spectrum of HgTe CQDs in the NIR range. (d) Raman spectrum. (e) Transmission electron microscopy image and histogram of synthesized QDs. (f) TEM image of larger area.
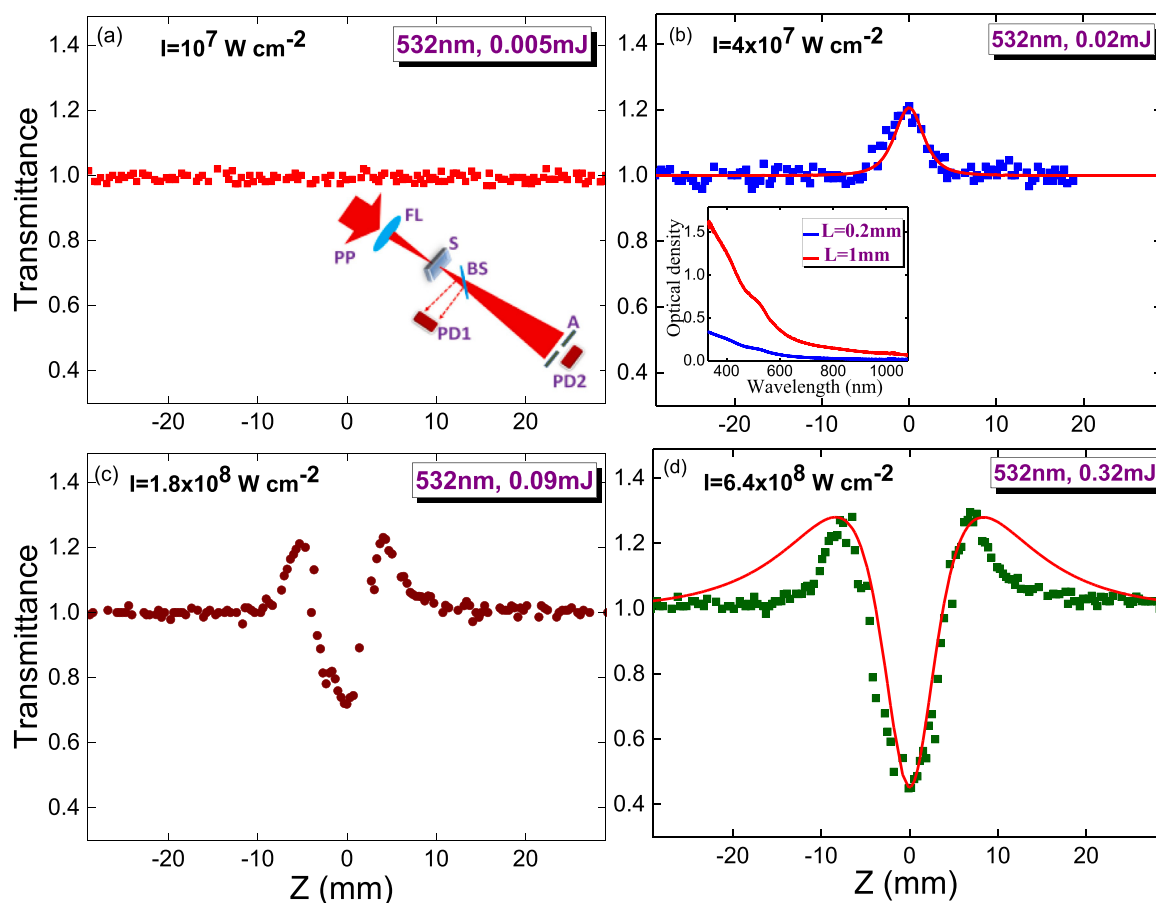

Fig. 2. Open-aperture Z-scans of 1-mm thick cell containing HgTe QD suspension using different energies of 532 nm, 10 ns pulses (a: 0.005 mJ; b: 0.02 mJ; c: 0.09 mJ; d: 0.32 mJ). The fittings are shown as solid curves in (b) and (d). Inset in Fig. 2a: Z-scan scheme. PP: probe pulse; FL: focusing lens; S: sample; BS: beamsplitter; A: aperture; PD1 and PD2: photodiodes for the measurements of open-aperture and closed-aperture data, respectively. Inset in Fig. 2b: Absorption spectra of the 0.2- and 1-mm thick cells containing HgTe QD suspensions ar 350 – 1080 nm.

closed-aperture (CA) scheme in order to recognize the sign and measure the nonlinear refractive index (γ) and open-aperture (OA) scheme in order to measure the nonlinear absorption coefficient (β). The working principle of z-scan technique is based on the motion of the sample along the z-axis from $-z$ to $+z$ through the focus of a tightly focused Gaussian laser beam. The motion of the sample across the focused beam exposes it to a varying irradiance (intensity) level reaching its maximum value at the focus point.

In most of experiments we used the second harmonic of the Nd:YAG laser (pulse duration 10 ns, pulse repetition rate 1 Hz) with $\lambda = 532$ nm obtained using a KDP crystal. We also used the fundamental radiation of this laser (1064 nm) for the studies of the optical nonlinearities of QDs in the near IR region. Laser radiation was focused with a 300 mm focal length spherical lens. The beam waist diameters were 80 μm and 60 μm (at half width of 1/e2 maximum of the spatial distribution at the focal plane) in the case of fundamental and second harmonic beams respectively. The 1-mm-thick fused silica cell containing HgTe QD colloidal suspension was moved along the z-axis through the focal point using a translating stage controlled by a computer. The energy of the laser pulse was measured using a calibrated photodiode and registered with a digital voltmeter. The energy of the pulses used in the experiment excluded the optical breakdown of the studied samples. The intensity of 532 nm radiation used in the experiments did not exceed 7×10^8 W cm^{-2}. The optical damage thresholds of suspensions using 10 ns, 532 nm and 10 ns, 1064 nm probe pulses were determined to be 6×10^9 and 9×10^9 W cm^{-2}, respectively. These values of optical damage were more than one order of magnitude larger than the intensities used during our measurements of the optical nonlinearities of samples.

Special attention was paid to the CA z-scans. To obtain them, the 1-mm aperture was fixed at a distance of 150 cm from the focal plane, behind which the second photodiode was located. The ratio of the transmitted radiation registered by the second photodiode and the incident radiation registered by the photodiode placed prior to the focusing lens was taken as the normalized transmission. Away from the focal point, where nonlinear processes do not occur, the normalized transmission was 1. This made it possible to avoid the influence of instability of the laser radiation on the results obtained. Each point on the experimental dependencies corresponds to an average of 20 measurements. The scheme with CA allowed determining the sign and value of the nonlinear refractive index of the QD-containing medium. The OA scheme allowed determination of the nonlinear absorption of the samples. The CA Z-scan scheme was calibrated using the known value of the nonlinear optical refraction of carbon disulfide. The error bars of the definition of the absolute values of nonlinear optical parameters were estimated to be $\pm 25\%$ due to the uncertainty in the measurements of the intensities of laser pulses in the focal plane.

The optical damage thresholds of suspensions using 10 ns, 532 nm and 10 ns, 1064 nm probe pulses were determined to be 6×10^9 and 9×10^9 W cm^{-2}, respectively. These values of optical damage were more than one order of magnitude larger than the intensities used during our measurements of the optical nonlinearities of samples.

The absorption spectra of 0.2- and 1-mm thick cells containing HgTe CQDs between 350 and 1080 nm are shown in the inset of Fig. 2b. The absorption coefficients of the used colloidal suspensions at 532 and 1064 nm were calculated to be 0.95 and 0.17 cm^{-1}, respectively. The standard fitting procedure was applied to the measured Z-scans, when commonly used relations for determination of the nonlinear refractive index, nonlinear absorption coefficients attributed to the 2PA (β_{2PA}), SA (β_{SA}), and RSA (β_{RSA}), as well as saturated intensity (I_{sat}), were used to fit our experimental data.

3.1. Nonlinear absorption

Fig. 2 shows the OA Z-scans of our sample using different intensities of 532 nm pulses. The intensities of pulses are shown on four separate graphs. Among different models determining the SA, which is a

dominant mechanism in the case of the weak probe pulses, are those describing by the two-level system possessing heterogeneously broadened states, kinetic model, and empirical model [14,15]. In the case of the kinetic model, the absorption coefficient can be presented as $\alpha(z) = \alpha_0/(1 + I(z)/I_{sat})$, where α_0 is the low-intensity linear absorption coefficient and $I(z)$ is the laser radiation intensity. This model showed the best fit with our experimental data (Fig. 2b, red solid curve). The relations of this model allowed determining the saturated intensity ($I_{sat} = 5 \times 10^8$ W cm^{-2}).

The corresponding negative nonlinear absorption coefficient was calculated to be $\beta_{SA} = -4 \times 10^{-9}$ cm W^{-1}. Our analysis showed that this parameter did not change with the growth of laser intensity in the range of 0.02 and 0.09 mJ energies of the 532 nm probe pulses. The application of 0.32 mJ pulses led to a decrease of β_{SA}, while the RSA dominated in the OA Z-scan (Fig. 2d). RSA started play an important role at the energies above 0.05 mJ (see the notable valley in the case of Z-scan using 0.09 mJ pulses (Fig. 2c). 2PA or RSA are the commonly reported mechanisms of the nonlinear absorption of QDs. In most cases, SA follows by RSA. HgTe CQDs show the absorption peak at 1412 nm (right inset in Fig. 2b). Taking into account the fact that we did not see the excitonic band attributed to QDs at the lower wavelengths of probe pulses (the absorption curve shown in Fig. 2b) one can assume that 2PA of 532 nm pulses hardly can be considered as an alternative to RSA mechanism of the positive nonlinear absorption observed in these studies. The fitting of Z-scan presented in Fig. 2d allowed determining β_{RSA} to be 1×10^{-8} cm W^{-1}.

The discrepancy between the fitting and experimental OA curves shown in Fig. 2d is probably attributed to some asymmetric (slightly elliptical) shape of the used beam in the focal area (see the discrepancy in the case of the negative and positive values of z). Similar discrepancies between theory and experiment were obtained in the case of other fittings performed during our studies. The corresponding error bars in the determination of the nonlinear optical parameters were estimated to be $\pm 30\%$.

We analyzed the possibility of dynamic scattering of the probe pulses in HgTe CQDs by installing additional photodiode out of the optical axis of beam propagation. These measurements showed the pattern of very weak and unchanged scattering during the propagation of our sample through the focal plane of the focusing lens while probing the whole range of used intensities of laser pulses. Thus, the nonlinear scattering cannot be considered as the mechanism of the decrease of normalized transmittance at the larger intensities of 532 nm probe pulses. The same conclusion was obtained in the case of twice longer wavelength of the probe pulses.

3.2. Nonlinear refraction

CA Z-scan studies were also carried out using different energies of the probe pulses. The following simplified equation can be used for calculation of the nonlinear refractive index of the sample at the conditions when the role of nonlinear absorptive effects becomes insignificant, like in the case shown in Fig. 3a: $\Delta T_{pv} \approx 0.4(1-S)^{0.25}|\Delta \Phi|$. Here ΔT_{pv} is the normalized difference between peak-to-valley transmission, S is the transmission of the aperture, $\Delta \Phi = k\gamma I_0 L_{eff}$, $k = 2\pi/\lambda$, λ is the radiation wavelength, I_0 is the laser radiation intensity in the focal plane, $L_{eff} = [1 - \exp(-\alpha L)]/\alpha$ is the effective length of the sample, α is the linear absorption coefficient, and L is the sample length. In the case shown in Fig. 3a the value of γ was determined to be -6×10^{-13} cm^2 W^{-1}.

In the case of $E = 0.02$ mJ when, apart from relatively moderate SA, only the negative nonlinear refraction plays an important role (Fig. 3b) one can exclude the positive nonlinear absorption from consideration. The fitting of the curve shown in Fig. 3b allowed determining γ and β_{SA} at $\lambda = 532$ nm (-7×10^{-13} cm^2 W^{-1} and -5×10^{-9} cm W^{-1}, respectively). These values were almost similar to the above-described measurements (-6×10^{-13} cm^2 W^{-1} and -4×10^{-9} cm W^{-1}, respectively).

The definition of the nonlinear refractive index of this suspension in
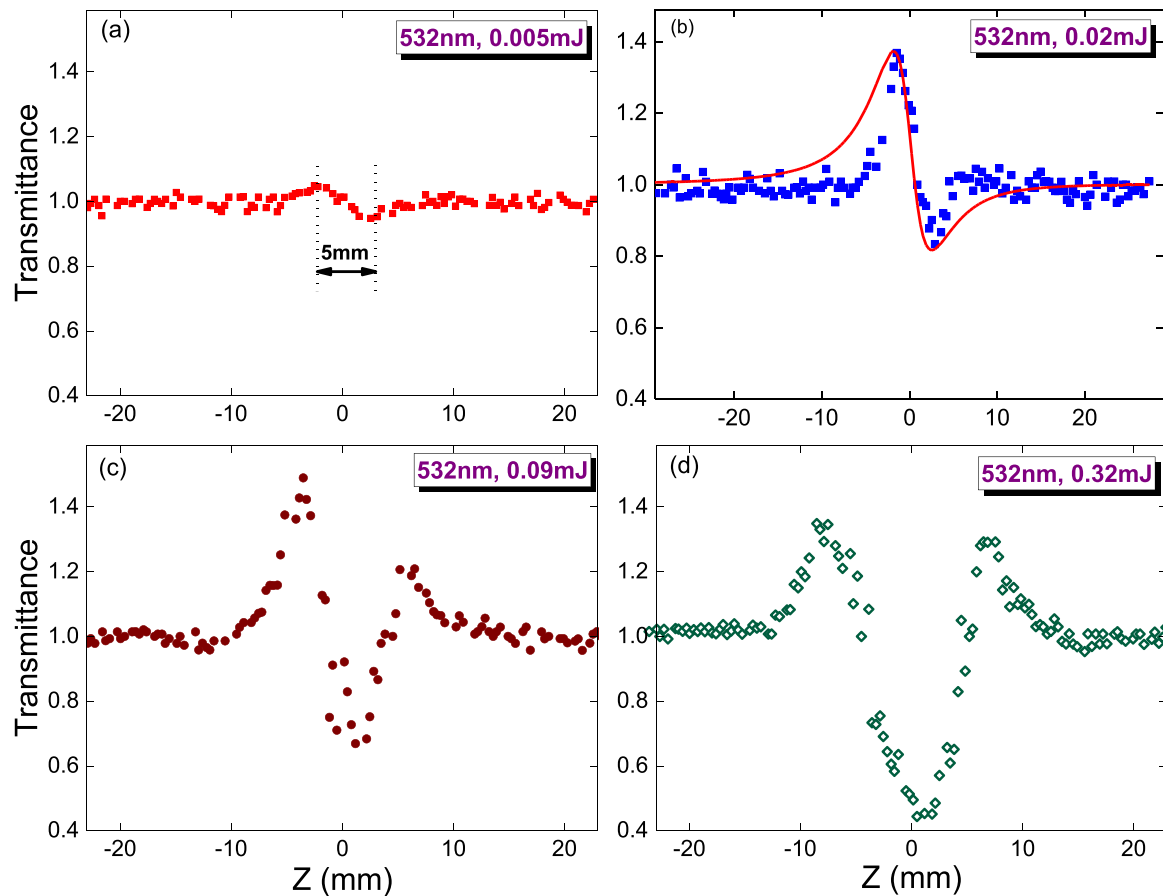
Fig. 3. Closed-aperture Z-scans of 1-mm thick cell containing HgTe QD suspension using different energies of 532 nm, 10 ns pulses (a: 0.005 mJ; b: 0.02 mJ; c: 0.09 mJ; d: 0.32 mJ). Solid curve in Fig. 3b shows the fitting with experimental data.

the case shown in Fig. 3c (E = 0.09 mJ) is a rather sophisticated procedure taking into account the necessity of fitting the experimental curve affected by three nonlinear optical processes in the case of relatively strong probe pulses: nonlinear refraction, SA, and RSA. The first and second processes can be manifested at weak pulses (0.005 and 0.02 mJ, Fig. 3a and 3b), while all three processes were inevitably presented in the CA Z-scan shown in Fig. 3c and especially in Fig. 3d.

In the case of 1064 nm, 10 ns pulses, we observed a reverse case of nonlinear absorption. Fig. 4 (green empty squares) shows the OA Z-scan using 0.85 mJ, 1064 nm, 10 ns pulses. The corresponding nonlinear absorption coefficient was derived from the fitting of this curve to be $\beta_{2PA} = 7 \times 10^{-10}$ cm W^{-1}. CA Z-scan showed the non-symmetric pattern attributed to the influence of 2PA (Fig. 4, red empty circles). Fitting of this curve using the relation comprising the joint manifestation of 2PA and nonlinear refraction allowed determining γ and β_{2PA} at this wavelength to be -5×10^{-14} cm^2 W^{-1} and 9×10^{-10} cm W^{-1}, respectively.

To confirm that the nonlinear optical properties are related to the HgTe QDs, the main solvent (tetrachloroethylene) was analyzed at two wavelengths (532 and 1064 nm) of probe radiation using similar procedure of Z-scan. No nonlinear optical response was observed during this test study, which indicated that the observed processes were derived entirely from HgTe QDs.

Another feature of small-sized species is their variable response related with the size effect, when the quantum confinement starts playing a decisive role in the case then the local field related effects enhance the nonlinear optical response of tiny particles, i.e. those which radius is less than the Bohr radius of the studied material. This is an interesting phenomenon; however, we did not analyze the nonlinear optical parameters for large particles, since the goal was to synthesize smallest (~4 nm) species and measure their nonlinear optical response.
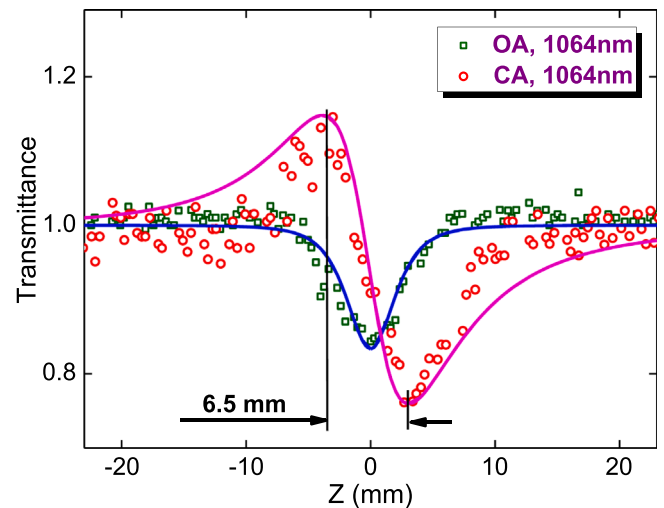
Fig. 4. Open-aperture (green empty squares) and closed-aperture (red empty circles) Z-scans of 1-mm thick cell containing HgTe QD suspension using 1064 nm, 0.85 mJ, 10 ns pulses ($I = 3 \times 10^9$ W cm^{-2}). Solid curves show the fittings of OA and CA data.(For interpretation of the references to colour in this figure, the reader is referred to the web version of this article.)

The dimensional effect in the nonlinear optical response of QDs, to the best of our knowledge, has not been studied for any of the known compositions due to the extreme complexity of interpreting the results. These are separate complex problems that do not have an obvious answer in advance, due to the fact that the type of nonlinearity with a

change in size can also be modified. This process depends on the fundamental properties of the nonlinear susceptibility of the substance under study, as well as on the structure of energy states in the QDs' band gap. With the change in size, their concentration and energy properties change. The laws according to which these changes occur are individual and require a comprehensive understanding of the dimensional effect of absorption. Some of the local centers can lead to nonlinear refraction, while others can lead to nonlinear absorption. To properly understand such a nonlinear response, it is necessary to define additional data using special techniques, such as photo- and thermo-stimulated luminescence.

Below, we compare the results of CA studies showing the self-defocusing of 532 nm and 1064 nm pulses. Our studies show that this process can be attributed to different physical mechanisms - Kerr effect and thermal effect. CA Z-scan at 532 nm probe pulses (Fig. 3a) shows a self-defocusing manifested with the peak preceding the valley, with the distance between them equal to 5 mm. This peak-to-valley distance in CA Z-scan becomes narrower compared with the conventional cubic process, with a separation corresponding to the relation $\Delta Z \approx 1.2z_0$, (z_0 is a Rayleigh length; it was equal to 4.2 nm for the 532 nm beam). In accordance with studies [16], such a relation can be attributed to the thermo-optical nonlinearity. Thus, we can attribute the observed process of self-defocusing in the studied QDs to the thermal effect while using the 532 nm, 10 ns pulses. Notice the absence of the thermal lens building in the pure tetrachloroethylene representing the main liquid component of the studied suspension.

In the case of Kerr-related nonlinearity, peak-to-valley distance has the following relation with the Rayleigh length of the focused radiation: $\Delta Z \approx 1.7z_0$. Such a relation was maintained in the case of 1064 nm pulses ($z_0 \approx 3.8$ mm) when Kerr-related nonlinearity showed a prevailing influence over the thermal-induced refractive nonlinearity (Fig. 4, $\Delta Z \approx 6.5$ mm). Additionally notice a very small absorption of CQD suspension at this wavelength, which prevents the formation of thermal lens. In this study, the application of 1064 nm, 10 ns pulses showed that the fast (electronic) nonlinearity leading to the negative nonlinear refractivity prevails over the slow (thermal) nonlinearity inducing the self-defocusing of propagated nanosecond pulse.

4. Discussion

When using the nanosecond pulses, there are thermal effects that can influence Z-scan profile. Obviously, when the nonlinear refraction appears to be negative, the researchers should be very careful to the generated thermal effects, which may be the main reason of the observed behavior. Particularly, one can argue that the distance between the minimum and the maximum of the CA Z-scan profile cannot unambiguously distinguish a thermal response from the one due to a Kerr effect. The Rayleigh length (z_0) can be poorly estimated and the uncertainty between $1.2z_0$ and $1.7z_0$ is too large to serve as a final criterion. We used different pulse repetition rates to analyze and exclude the role of accumulative thermal lens formation during these studies. Our studies at 1 and 10 Hz pulse repetition rates did not show a difference in the CA Z-scans. Thus the accumulative thermal effect can be excluded from the consideration for both wavelengths (532 and 1064 nm). Next, the analysis of the 1064 nm pulse shape after propagation of the studied sample did not reveal the change of the trailing part of pulses, which is a sign of the absence of the dynamic thermal effect. That is why we used only the Kerr effect mechanism to characterize our experimental results of the nonlinear refractive properties of HgTe QD suspension in the case of 1064 nm probe pulses. Meanwhile, some variation of the trailing part of 532 nm pulses leading to the sharper drop of intensity and narrowing of the pulse duration may point out the influence of the dynamic thermal lens appearance. Below we address this effect in the case of the studied QD suspension, which corroborated with conclusion about the influence of thermal effect using the analysis of the distance between peak and valley in the CA Z-scan.

The nonlinear contribution to the refractive index at appropriate

experimental conditions can also be due to the thermal effect. This effect consists of two parts: one is the "fast" process of acoustic wave propagation, and other is the "slow" steady state changing of medium density due to accumulative thermal heating of the absorbing area. The slow process should be taken into consideration at low thermal conductivity and/or high pulse repetition rates, which did not coincide with the conditions of the discussed experiments. The fast process causes the matter density variations due to acoustic wave propagation after local heating. Thus this process can be a reason of the observed CA Z-scan in the case of 532 nm pulses absorbing in the suspension.

The rise time (τ), which is necessary for observing the density variations and further the refractive index variations, is determined by a ratio of beam waist radius at the focal point to the sound velocity in the medium ($\tau = w_0 / V_s$). Taking into account our experimental conditions ($w_0 = 30$ µm for 10-ns pulses at the wavelength of 532 nm, $V_s \approx 1600$ m/s), a rise time can be estimated as ~20 ns, i.e., the influence of the thermal effect should not be entirely neglected in the case of 10 ns pulses.

The technique previously proposed to reveal a slow nonlinear mechanism in Z-scan-like γ measurements [17] was based on the analysis of the temporal waveform of the beam transmitted through an aperture in the CA Z-scan scheme. The trailing part of the radiation self-defocuses inside the cell when the intensity reaches its definite value at the appropriate point of the Z scale. As a result, the smaller part of the whole radiation passes through the aperture and registers by a fast registrar. Thus, the type of nonlinearity can be estimated by analyzing the variations of temporal shape of propagated pulse when the sample placed at the peak or valley position of the Z-scan.

The variation of the trailing part of 532 nm pulses leading to the sharper drop of intensity and narrowing of the pulse duration observed during these studies underlines the appearance of the acoustic thermal lens. The variation of waveform indicates the manifestation of transient negative nonlinear refraction induced by the acoustic wave. This peculiarity, as well as the distance between the maximum and minimum positions of CA Z-scan, which appeared to be shorter than $1.7z_0$, confirms the assumption of the involvement of linear absorption induced process of the acoustic wave formation leading to the negative nonlinear refraction of HgTe QD suspension.

Chalcogenides are known to be fragile materials even at low intensities in linear regime. It is difficult to characterize them without photo inducing damages especially at 532 nm where the absorption is relatively high. To study at the conditions when the QDs are not destroyed, we did not used large intensity of the probe pulses used for Z-scans.

Another problem occurring in the case of nanosecond pulses in presence of absorbing material, which is the case of 532 nm probe emission, is a formation of bubble growth with heat and diffusion of the light outside the photodiode [18]. This method allowed earlier detecting the dynamic scattering of laser radiation in silver nanoparticles suspensions, which manifested by the formation of a symmetric dip in the OA Z-scan when samples with nanoparticles approach the focal plane [19]. We tested this possibility of the nonlinear scattering by putting an additional photodiode out of the propagation axis and did not find this process while changing the intensity of the probe 532 nm pulses.

Recently, the measurements of the saturated intensities, saturable absorption, and nonlinear refraction in the 70 nm thick films containing 4 nm HgTe QDs using short laser pulses were reported [8]. The strong nonlinear refraction and saturable absorption in the thin films containing HgTe QDs using the tunable 28 ps and 150 fs pulses were demonstrated. Those studies were carried out using the tunable laser pulses (400 – 1100 nm). The maximal values of the nonlinear absorption coefficients and nonlinear refractive indices determined along the studied wavelength range were -2.4×10^{-5} cm^2 W^{-1} (in the case of 28 ps, 700 nm probe pulses) and -3×10^{-9} cm^2 W^{-1} (in the case of 28 ps, 400 nm probe pulses), respectively. No RSA was observed in two cases of short laser pulses, contrary to the case reported in present study

using the 532 nm, 10 ns probe pulses. Once comparing the results of measurements of the nonlinear absorption attributed to the SA one can admit a significant growth of this parameter in the case of 28 ps pulses and thin HgTe QD film with regard to the liquid phase of these QDs analyzed using long (10 ns) pulses. The optical densities in these two cases were approximately the same, so the reason in such a difference in β_{SA} (-4×10^{-9} cm W^{-1} in the case of the 532 nm, 10 ns probe pulses and -2.4×10^{-5} cm W^{-1} in the case of the 700 nm, 28 ps probe pulses) can be attributed to the significantly larger cross-section of this process in the latter case. Meanwhile, the saturated intensity in the case of 10 ns pulses ($I_{sat} = 5 \times 10^{8}$ W cm^{-2}) was lower compared with the shorter probe pulses (7 $\times 10^{9}$ and 4 $\times 10^{10}$ W cm^{-2} in the case of 28 ps and 150 fs pulses, respectively). Low-I_{sat} saturable absorbers may allow formation of the low-threshold femtosecond laser sources. As for the measurements of nonlinear refraction, the difference in γ (-7×10^{-13} cm^2 W^{-1} and -3×10^{-9} cm^2 W^{-1} in the case of 10 ns, 532 nm and 28 ps, 400 nm probe pulses, respectively) can be caused by the involvement of different processes (the thermal lens effect and the Kerr effect enhanced in the vicinity of the absorption band of QDs). In the case of picosecond pulses, the molecular Kerr-related nonlinearities of chalcogenides can notably prevail over the electronic Kerr-related process.

5. Potential applications of mercury telluride quantum dots in nonlinear optics and optoelectronics

Recent studies of different groups show that various emerging types of nonlinear optical materials, such as few-layer tin sulfide, few-layer bismuthene, graphdiyne, etc., show interesting nonlinear optical response. Particularly, in [20], as an analogue compound of black phosphorus, a new 2D semiconducting few-layer SnS was successfully synthesized, and its nonlinear optical response is investigated. It was shown that its nonlinear refractive index and third-order nonlinear susceptibility are measured as 10^{-5} cm^2 W^{-1} and 10^{-10} esu, respectively. By taking advantage of such a large Kerr nonlinearity, an all-optical switching technique based on few-layer SnS was realized through modulating the propagation of the signal beam by another controlling beam. In [21], the broadband nonlinear optical properties and carrier dynamics of the tin sulfide, a novel two-elemental and 2D structural black phosphorus analog monochalcogenide have been systematically investigated via *Z*-scan and transient absorption approaches. The nonlinear absorption coefficient of 50.5 × 10^{-3} cm/GW^{-1} order of magnitude larger than that of BP, endows the promising application of SnS in ultrafast laser generation. Bismuthene has received tremendous interests owing to its advantages in electronic-transport, semimetallic bonding, and intrinsic spin-orbit coupling. The nonlinear optical absorption and refraction parameters of this material had been characterized by laser Z-scan and spatial phase modulation measurement techniques, respectively [22]. The achievement of all optical switching suggests that the bismuthene-based 2D material is an excellent candidate for an all optical switcher. Graphdiyne is a new carbon allotrope comprising sp- and sp^2-hybridized carbon atoms arranged in a 2D layered structure. In this contribution, 2D graphdiyne is demonstrated to exhibit a strong light–matter interaction with high stability to achieve a broadband Kerr nonlinear optical response, which is useful for nonreciprocal light propagation in passive photonic diodes. Graphdiyne has been studied in [23] and demonstrated a large nonlinear refractive index in the order of $\approx 10^{-5}$ cm^2 W^{-1}, comparing favorably to that of graphene.

It is difficult to compare those structures with our samples. Each of them shows their positive and negative properties. Meanwhile, the practical application of different materials depends on the requirements to some concrete tasks.

Quantum dots of mercury telluride have great prospects for application in passive mode-lockers and optical switches in the fiber data transmission lines. Due to the possibility of tuning resonances in absorption and luminescence ranges, these QDs cover the entire

wavelength range (from 1260 nm to 1625 nm) where the fiber data transmission lines are most perspective. The most of scientific and commercial interest to mercury quantum dots arises from the semimetal nature of bulk HgTe material [1]. Almost zero band gap in quantum dots alongside the tunable absorption/emission in near-/far-IR are among the attractive properties of HgTe QDs. Currently, HgTe QDs with absorption from 1 up to 12 micrometers are reported. Generally, it is expected that HgTe QDs could replace the expensive epitaxialy-grown mercury cadmium telluride in sensors, spectrometers, and so on [2,24].

Colloidal nanocrystals can be used for the construction of infrared devices such as photodetectors, mid-infrared cameras, multispectral detectors, and low-threshold lasers [25–29]. Below we are addressing another potential application of HgTe nanocrystals. The goal of present study is a determination of the low-order optical nonlinearities of mercury telluride quantum dots. One can consider a connection between them and higher-order nonlinear optical response of material. In particular, the high-order harmonics can efficiently generate in the media containing the quantum dots possessing strong nonlinear refraction and absorption. Notice that previous studies of the QDs showed the notable enhancement of harmonic yield compared with the case when high-order harmonics generation (HHG) was carried out in the plasmas produced on the surfaces of bulk silver sulfide, zinc sulfide, and alloyed cadmium-zinc sulfide [30]. Correspondingly, high-order harmonics generation could be a potential area of future applications of this material.

Tunable absorption/emission in near-/far-IR of HgTe CQDs make them the most promising for applications in photoconductive, photovoltaic, and phototransistor devices, plasmon assisted photodetection, multicolor detection, etc. In addition to above potential applications, QDs HgTe can be widely used in such areas as photonics, quantum sensors, etc. Currently, extensive research is underway on this material as the basis of IR radiation detectors in a wide range of wavelengths [31].

We would also like to underline that the difference in the measurements of the low-order nonlinearities attributed to the application of the lasers of different pulse width does not change the conclusion about the relative magnitudes of the nonlinear optical parameters since the refereed studies used both nanosecond and femtosecond pulses. Thus, one can expect the high level of harmonic yield in the case HgTe QDs. The synthesized HgTe QDs yet treated as the medium for HHG. The confirmation of above assumption will support the conclusion about the connection of different types of optical nonlinearities. Notice that even being a medium showing the moderate level of HHG efficiency, these QDs will be more useful compared with the molecular/ionic HgTe species or large HgTe nanoparticles. This statement is not an assumption but rather a rule confirmed in numerous plasma and gas HHG experiments when small-sized agglomerates allow the larger harmonic yield compared to the molecular species of the same elemental consistency.

6. Conclusions

In conclusion, we have synthesized the colloidal mercury telluride quantum dots and analyzed their low-order nonlinear optical properties using 1064 nm and 532 nm, 10 ns pulses. HgTe QDs colloidal suspension have shown the strong nonlinear absorption and negative nonlinear refraction (saturation intensity $I_{SA} = 5 \times 10^{8}$ W cm^{-2}, nonlinear absorption coefficients attributed to the saturable absorption and reverse saturable absorption $\beta_{SA} = -4 \times 10^{-9}$ cm W^{-1} and $\beta_{RSA} = 1 \times 10^{-8}$ cm W^{-1}, nonlinear refractive index $\gamma = -6 \times 10^{-13}$ cm^2 W^{-1}) while using the 532 nm probe pulses. The nonlinear optical parameters of this suspension at 1064 nm were smaller (nonlinear absorption coefficient attributed to the two-photon absorption $\beta_{2PA} = 6 \times 10^{-10}$ cm W^{-1}, $\gamma = -5 \times 10^{-14}$ cm^2 W^{-1}) compared with the case of 532 nm probe pulses. The negative nonlinear refraction of HgTe QDs was attributed to the thermal and Kerr effects in the case of 532 nm and 1064 nm probe pulses, respectively.

Funding

CRediT authorship contribution statement

R. A. Ganeev: Supervision, Conceptualization, Writing – review & editing. **I. A. Shuklov**: Methodology, Investigation. **A. I. Zvyagin**: Investigation. **A. Mardini**: Investigation. **A. A. Lizunova**: Investigation. **O. V. Ovchinnikov**: Methodology, Investigation. **G. S. Boltaev**: Investigation. **I. B. Sapaev**: Investigation. **V. V. Kim**: Investigation. **V. F. Razumov**: Methodology, Investigation.

Declaration of Competing Interest

The authors declare that they have no known competing financial interests or personal relationships that could have appeared to influence the work reported in this paper.

Data Availability

The data that support the findings of this study are available on request from the corresponding author.

Acknowledgement

References

[1] C. Gréboval, A. Chu, N. Goubet, C. Livache, S. Ithurria, E. Lhuillier, Chem. Rev. 121 (2021) 3627–3700.

[2] P. Wang, H. Xia, Q. Li, F. Wang, L. Zhang, T. Li, P. Martyniuk, A. Rogalski, W. Hu, Small 15 (2019), 1904396.

[3] A. Al-Otaifya, S.V. Kershaw, S. Gupta, A.L. Rogach, G. Allan, C. Delerue, D.J. Binks, Phys. Chem. Chem. Phys. 15 (2013) 16864–16873.

[4] S.B. Brichkin, V.F. Razumov, Russ. Chem. Rev. 85 (2016) 1297–1312.

[5] A. Shuklov, V.F. Toknova, A.A. Lizunova, V.F. Razumov, Mater. Today Chem. 18 (2020), 100357.

[6] A. Shuklov, V.F. Razumov, Russ. Chem. Rev. 89 (2020) 379–391.

[7] P.A. Wolff, S.Y. Yuen, K.A. Harris, J.W. Cook Jr., J.F. Schetzina, Appl. Phys. Lett. 50 (1987) 1858–1957.

[8] A. Bundulis, I.A. Shuklov, V.V. Kim, A. Mardini, J. Grube, J. Alnis, A.A. Lizunova, V.F. Razumov, R.A. Ganeev, Nanomater 11 (2021) 3351.

[9] I.A. Shuklov, I.S. Mikhel, A.V. Nevidimov, K.P. Birin, N.V. Dubrovina, A. A. Lizunova, V.F. Razumov, Chem. Sel. 5 (2020) 11896–11900.

[10] S. Keuleyan, E. Lhuillier, P. Guyot-Sionnest, J. Am. Chem. Soc. 133 (2011) 16422–16424.

[11] N. Goubet, A. Jagtap, C. Livache, B. Martinez, H. Portalès, X.Z. Xu, R.P.S.M. Lobo, B. Dubertret, E. Lhuillier, J. Am. Chem. Soc. 140 (15) (2018) 5033–5036.

[12] M.V. Kovalenko, E. Kaufmann, D. Pachinger, J. Roither, M. Huber, J. Stangl, G. Hesser, F. Schaeffler, W. Heiss, J. Am. Chem. Soc. 128 (2006) 3516–3517.

[13] G. Allan, C. Delerue, Phys. Rev. B 86 (2012) 165437.

[14] L. Yang, R. Dorsinville, Q.Z. Wang, P.X. Ye, R.R. Alfano, R. Zamboni, C. Taliani, Opt. Lett. 17 (1992) 323–325.

[15] M. Samoc, A. Samoc, B. Luther-Davies, H. Reisch, U. Scherf, Opt. Lett. 23 (1998) 1295–1297.

[16] M. Falconieri, G. Salvetti, Appl. Phys. B 69 (1999) 133–136.

[17] H. Toda, C.M. Verber, Opt. Lett. 17 (1992) 1379–1381.

[18] L. Vivien, D. Riehl, J.-F. Delouis, J.A. Delaire, F. Hache, E. Anglaret, J. Opt. Soc. Am. B 19 (2002) 208–214.

[19] A.I. Zvyagin, A.S. Perepelitsa, M.S. Lavlinskaya, O.V. Ovchinnikov, M.S. Smirnov, R.A. Ganeev, Optik 175 (2018) 93–98.

[20] L. Wu, Z. Xie, L. Lu, J. Zhao, Y. Wang, X. Jiang, Y. Ge, F. Zhang, S. Lu, Z. Guo, J. Liu, Y. Xiang, S. Xu, J. Li, D. Fan, H. Zhang, Adv. Opt. Mater. 6 (2018), 1700985.

[21] Z. Xie, F. Zhang, Z. Liang, T. Fan, Z. Li, X. Jiang, H. Chen, J. Li, H. Zhang, Phot. Research 7 (2019) 494–502.

[22] L. Lu, W. Wang, L. Wu, X. Jiang, Y. Xiang, J. Li, D. Fan, H. Zhang, ACS Photon 4 (2017) 2852–2861.

[23] L. Wu, Y. Dong, J. Zhao, D. Ma, W. Huang, Y. Zhang, Y. Wang, X. Jiang, Y. Xiang, J. Li, Y. Feng, J. Xu, H. Zhang, J. Adv. Mater. 31 (2019), 1807981.

[24] A. Rogalski, Rep Prog, Phys 68 (2005) 2267.

[25] M. Chen, X. Lan, X. Tang, Y. Wang, M.H. Hudson, D.V. Talapin, P. Guyot-Sionnest, ACS Photonics 6 (2019) 2358.

[26] K. Liu, X. Xu, W. Shan, D. Sun, C. Yao, W. Sun, Opt. Mater. 99 (2020), 109569.

[27] P. Rastogi, A. Chu, T.H. Dang, Y. Prado, C. Gréboval, J. Qu, C. Dabard, A. Khalili, E. Dandeu, B. Fix, X. Zhen, Xu, S. Ithurria, G. Vincent., B. Gall., E. Lhuillier, Adv. Opt. Mater. 9 (2021), 2002066.

[28] M. Chen, H. Lu, N.M. Abdelazim, Y. Zhu, Z. Wang, W. Ren, S.V. Kershaw, A. L. Rogach, N. Zhao, ACS Nano 11 (2017) 5614.

[29] X. Tang, X. Tang, K.W.C. Lai, ACS Photonics 3 (2016) 2396–2404.

[30] R.A. Ganeev, G.S. Boltaev, V.V. Kim, K. Zhang, A.I. Zvyagin, M.S. Smirnov, O. V. Ovchinnikov, P.V. Redkin, M. Wöstmann, H. Zacharias, C. Guo, Opt. Express 26 (2018) 35013–35025.

[31] C. Melnychuk, P. Guyot-Sionnest, J. Electron. Mater. 51 (2022) 1428–1435.